Correction of shallow-water electromagnetic data for noise induced by instrument motion

Pamela F. Lezaeta[1], Alan D. Chave[1], and Rob L. Evans[1]

ABSTRACT

An unexpected noise source has been found in magnetic- and sometimes electric-field data recorded on the bottom of lakes in the Archean Slave craton (northwestern Canada) during warm seasons. The noise is the result of instrument motion and in some instances direct induction by wind-driven surface gravity waves when the lakes are not ice covered. The noise can be reduced or eliminated by prefiltering the data with an adaptive correlation noise-canceling filter using instrument tilt records prior to estimation of magnetotelluric (MT) response functions. Similar effects are to be expected in other shallow-water environments, and the adaptive correlation canceler is a suitable method to preprocess MT data to reduce motion-related noise in the magnetic field. This underscores the importance of ancillary tilt measurements in shallow-water MT surveys. In coastal or lake-bottom surveys, special efforts to reduce hydrodynamic effects on the instrument should also be pursued.

INTRODUCTION

Between 1998 and 2000, two magnetotelluric (MT) surveys were conducted on the Archean Slave craton in 18 lakes during 19 deployments using continental shelf electromagnetic (EM) instrumentation designed for use at depths less than 1000 m (Petitt et al., 1994). The instruments were deployed from float airplanes during the ice-free summer months and were retrieved the following summer. The first sequence of lakes was surveyed for 11 months, at which point the instruments were retrieved and transferred to a second series of lakes for another year. The measurements were aimed at determining the regional-scale 3D electrical structure of the craton (Jones et al., 2003).

During the first month of each survey, the data were recorded at a high sample rate (1.75 s) for imaging crustal features. The instruments then switched automatically to a lower sample rate (28 s) for the remainder of the deployment to obtain long-period MT data, permitting deep penetration into the lithospheric mantle and below. Each instrument was programmed to record the time variations of the two orthogonal horizontal electric fields across a 3-m span using silver–silver chloride (Ag-AgCl) electrodes, and the three-component magnetic-field variations were measured using a suspended magnetic sensor (Filloux, 1987). The horizontal-plane tilt variations of the cylindrically shaped magnetometer pressure case were also measured with microradian resolution. Figure 1 shows an instrument being deployed. Instrument installation depths ranged from 7 to 50 m, with 15 to 20 m being a typical value.

Time series of tilt and magnetic field were stable in winter except for normal geomagnetic variations; they displayed strongly disturbed intervals from late spring through summer and into early fall. The disturbance was particularly noticeable in the high-sample-rate data, where short-period tilt variability correlated strongly with the magnetic-field (and sometimes the electric-field) fluctuations. Such noise was somewhat unexpected because the lakes were believed to be calm with weak water currents in comparison to the continental shelves.

This paper focuses on (1) the analysis of nonstationary instrument motion that affected the magnetic-field (and sometimes the electric-field) data and on (2) the development of a time-domain mitigation technique for the correlated noise using an adaptive correlation cancellation filter prior to estimation of frequency-domain MT response functions. We also propose a physical explanation for the cause of the instrument motion and suggest a possible means to minimize the problem.

DATA SET

Figure 2 shows the location of the lake-bottom sites. In the first survey, from August 1998 to August 1999, ten sites were recorded; nine more sites were occupied during the second year, from September 1999 to August 2000.

The electric and magnetic channels were edited to correct for obvious instrument effects (such as infrequent data spikes

and regular magnetic-field calibration pulses) and high-pass filtered to remove long-term drift using a fourth-order Butterworth filter having a 24 000-s cutoff period run forward and backward across the data to eliminate possible phase shifts. Because of inevitable and uncontrollable electrode drift, the
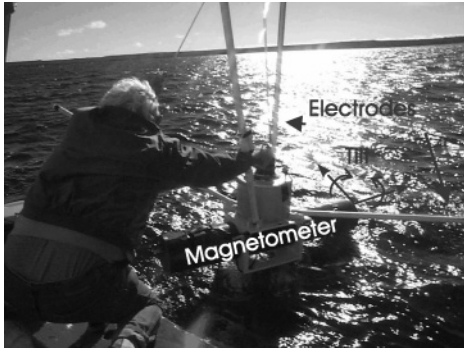

Figure 1. A sea-floor instrument used in the lake-bottom surveys on the Slave craton being deployed from an Otter twin-engine floatplane. Arrows indicate the parts of the instrument; the electrodes (at the ends of the two orthogonal light plastic pipes) are above the magnetometer and tilt sensor inside a horizontal cylindrical aluminum pressure case. Tilt is the angular deflection of the two horizontal principal coordinates of the cylinder, and the magnetometers are rotated by 45° from the horizontal electrode pipes. The tripod anchor for the instrument is underwater.
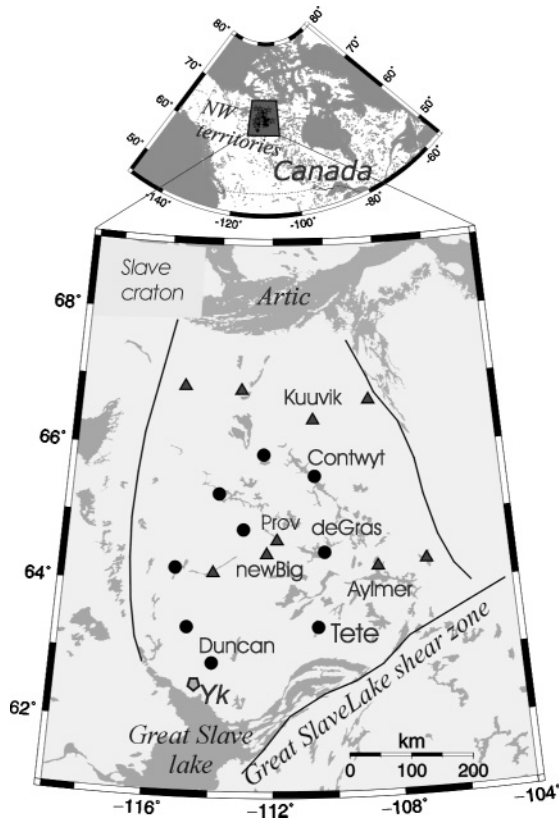

Figure 2. Location of MT stations deployed on the bottom of lakes in the Slave craton (northwestern Canada). Black dots and triangles are sites from the first- and second-year surveys, respectively. YK is the Yellowknife weather station. The inset above shows a regional map of Canada.

two electric channels occasionally were out of range even with gain ranging applied, producing some data gaps in one or both components. The magnetic time series were continuous. Figure 3 shows examples of magnetic and electric time variations from Newbigging Lake (newBig in Figure 2) for a ten-hour window at the high (1.75-s) sample rate. During the first six hours, the data have a higher frequency character than during subsequent hours, particularly for the magnetic field. The magnetic-field and tilt variations approximately covary during the first six hours of the window (Figure 4). Many sites
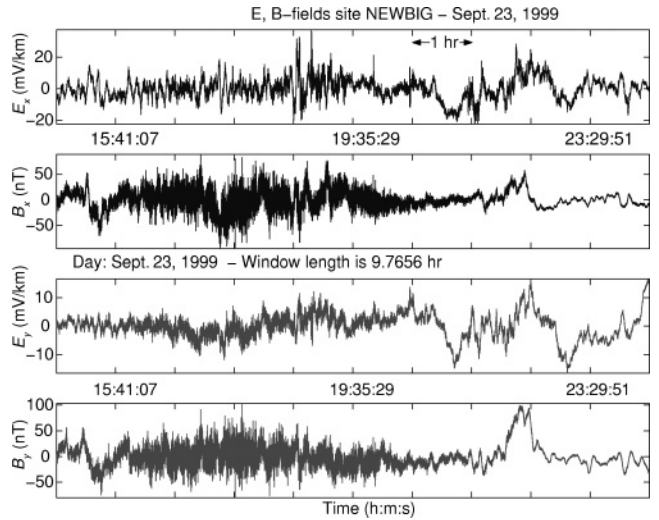

Figure 3. Ten-hour window of the time series from Newbigging Lake (see Figure 2 for location) at a sample interval of 1.75 s for September 23, 1999. The two graphs at the top illustrate the original x-component of the electric (E_x) and magnetic (B_x, along the magnetometer cylinder) channels. The two bottom graphs show the corresponding perpendicular y-component of the fields. The E fields are at 45° with respect to B.
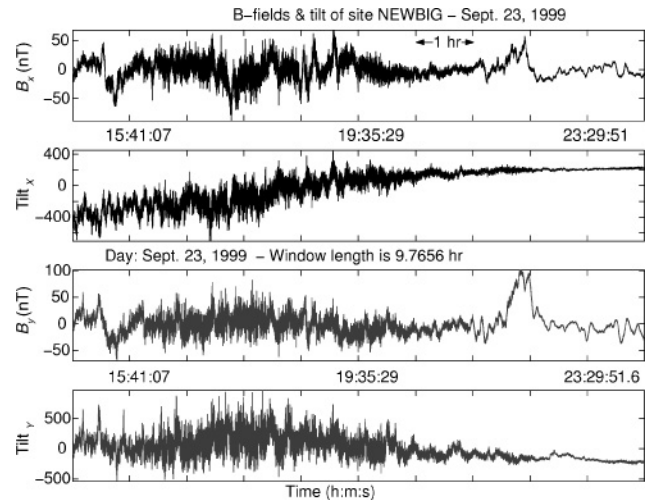

Figure 4. Ten-hour window of magnetic-field and tilt-time variations from Newbigging Lake (see Figure 2 for location) at a sample interval of 1.75 s for September 23, 1999. The four traces from top to bottom illustrate the horizontal x-component of the magnetic field (B_x) and tilt (Tilt$_x$) and the y-component B_y and Tilt$_y$, respectively. Tilt is in microradians. The horizontal components are as for Figure 3.

displayed similar correlations in the high-sample-rate time series during the summer months.

TILT NOISE CORRELATION
WITH FIELD COMPONENTS

The corresponding components of tilt and magnetic field vary coherently when the high-frequency disturbance is present. This disturbance was generally at least twice as large for the y-component across the magnetometer cylinder compared to the along-cylinder x-component. Although not truly periodic, the variations have a dominant period of about 4.5 s, which becomes clear for short time windows (Figure 5). The electric field E is usually not correlated with the disturbed tilt except in extreme cases. Figure 6 shows an example of this exception for the y-component from Newbigging Lake; the E_x field seems unaffected by the tilt motion (Figure 6, top). The electric-field perturbation when present lasted from a few minutes to as long as several hours, also with a period of approximately 4.5 s.

It is well known that mechanical motion of a magnetometer in the earth's magnetic field will generate an apparent magnetic field (e.g., Bastani and Pedersen, 1997) and hence correlated noise, but this should not affect the electric field unless $\mathbf{v} \times \mathbf{B}$ is comparable to the ambient field and there is local induction in the surrounding medium, as occurs in the highly conductive ocean for a variety of water disturbances. Further discussion is presented in a later section.

Power spectra for the magnetic field and tilt computed from perturbed and quiet time segments (Figure 7) show that tilt motion systematically affected the magnetic field at periods below 1000 s, with peak amplitudes centered below 10 s (Figure 7), consistent with the time series plots. During disturbed times, the high-frequency magnetic-field noise floor rose by up to four decades in power, consistent with the change for tilt. The tilt motion also systematically affected the vertical magnetic-field component by around one to two decades in

power, while it was not significant in the power spectrum of the electric-field components for most of the sites.

NOISE REMOVAL WITH AN ADAPTIVE
CORRELATION CANCELLATION FILTER

Tilt-induced noise is highly variable in time; hence, removal using frequency-domain transfer function methods implicitly dependent on the stationarity assumption are of little use. Time-domain data adaptive-filtering methods have been developed that are applicable to nonstationary situations, of which the most useful in the present context is the
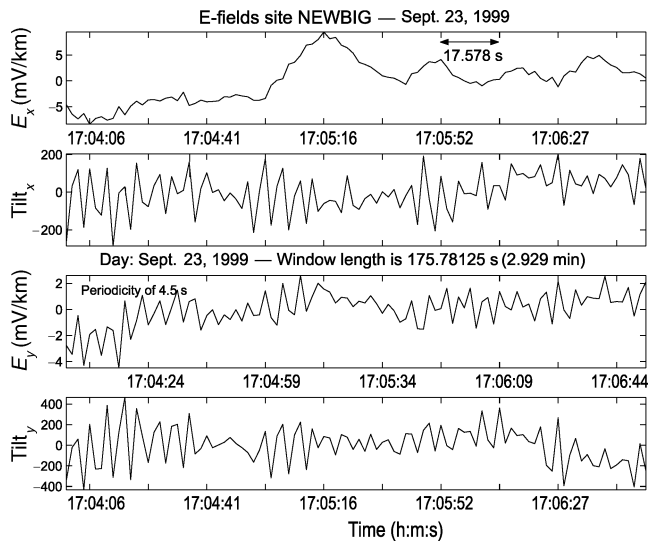

Figure 6. Three-minute window of the electric-field (in the measurement coordinate system) and tilt-time variations from Newbigging Lake (see Figure 2 for location) at a sample interval of 1.75 s for September 23, 1999. The four traces from top to bottom illustrate the horizontal components as for Figure 4.
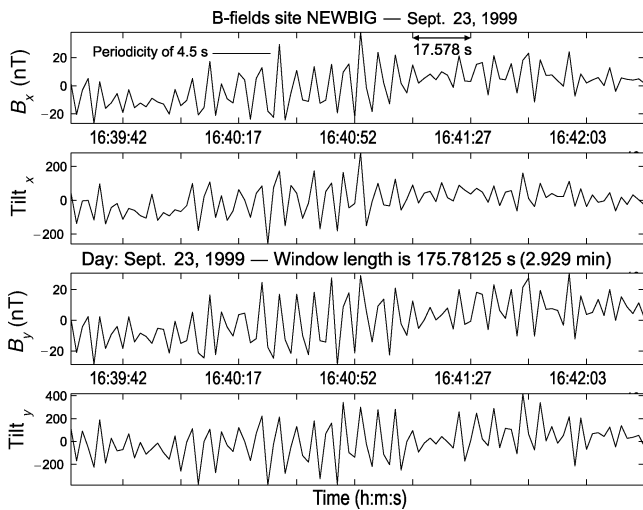

Figure 5. Three-minute window of magnetic-field and tilt-time variations from Newbigging Lake (see Figure 2 for location) at a sample interval of 1.75 s for September 23, 1999. The four traces from top to bottom illustrate the horizontal components as for Figure 4.
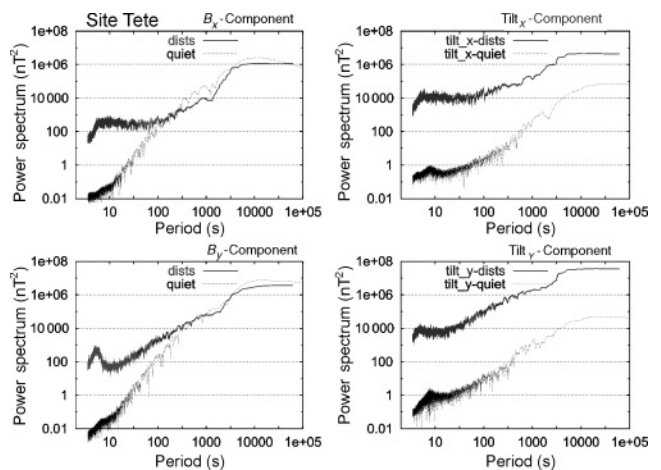

Figure 7. Power spectra as a function of period for the magnetic-field components B_x and B_y (left) and the tilt components x and y (right) for Lake Tete d'Ours. The two curves in each plot correspond to the power spectra from highly disturbed (dists) (August 11–12, 1998) and relatively quiet tilt-time segments (August 7–10, 1998).

adaptive-correlation canceler (Widrow and Stearns, 1994). The adaptive-correlation canceler incorporates time-variable filter coefficients that change in an optimal sense to remove unknown interference contained in a primary signal, using a noise reference in which the primary signal is weak or nonexistent (Figure 8). In our study, the primary contaminated signal is a component of the magnetic (or sometimes electric) field, and the reference (noise) signals are the two horizontal components of tilt. Each adaptive filter is a linear transversal (finite-impulse response) filter whose coefficients are updated at each time step using the least-mean-square (LMS) algorithm.

Let the primary signal S be given by

$$S = S_o + n_o, \tag{1}$$

where n_o represents the noise in S that is correlated in an unknown manner with the corrupted signals or reference noise $Ref1$ and $Ref2$ (i.e., the two tilt components). The signal free of such noise is thus given by S_o.

At the discrete time m, let the predicted noise $\mathbf{y}(m)$ be the sum of the outputs of the adaptive filters, let the adaptive filter coefficients be $W1(m)$ and $W2(m)$, and let the reference signals be $Ref1(m)$ and $Ref2(m)$ (Figure 8). The output of the adaptive filter at time m is

$$\mathbf{y}(m) = W1(m) \times Ref1(m) + W2(m) \times Ref2(m)$$
$$= \mathbf{W}(m) \times \mathbf{Ref}(m). \tag{2}$$

Using the LMS algorithm, at time step $m+1$ the filter (the matrix $\mathbf{W}$ in equation 2) is given by

$$\mathbf{W}(m+1) = \mathbf{W}(m) + \frac{\mu \times \mathbf{err}(m) \times \mathbf{Ref}(m)^t}{\alpha + \sum_{i=1}^{N} \mathbf{Ref}(m-i)^2}, \tag{3}$$

with the superscript t representing the transpose of the matrix $\mathbf{Ref}$ and N the filter length. The coefficient μ is the adaption step size of the time-domain filter and α is a damping factor, both of which are found iteratively by minimizing the sum of squared differences between the input data and the predicted noise [$\mathbf{err}^2(m)$; equation 4] over the time space of input data m ($m = 1, \ldots, Nd$, where Nd is the number of data points). The

output signal at the discrete time m is the difference between the primary input signal $\mathbf{X\_in}$ delayed by a given time ($N/2$) and the filter output signal $\mathbf{y}(m)$:

$$\mathbf{err}(m) = \mathbf{X\_in}\left(m - \frac{N}{2}\right) - \mathbf{y}(m), \tag{4}$$

where $N/2$ is a delay time introduced to grow the coefficients toward the center of the filter ($\mathbf{W}$ in equation 3), so that if timing between the input primary signal $\mathbf{X\_in}(m)$ and the reference noise $\mathbf{Ref}$ is not aligned, the correlator $\mathbf{W}$ will be able to find the correct value (within the interval $\pm N/2$ of the filter length N). The starting set of adaptive filters $\mathbf{W}(m)$ (i.e., for $m = 1, \ldots, N$) are initialized to zero at a first step (each step is over the time space Nd of input data). For further steps, $\mathbf{W}$ will start from the previous result, computing the following $\mathbf{W}(m)$ as in equation 3 to result in the output $\mathbf{err}(m)$ (equation 4) from the sum of predicted noise (equation 2) over the filter length N:

$$\mathbf{y}(m) = \sum_{i=1}^{N} \mathbf{W}(m-i)\mathbf{Ref}(m-i). \tag{5}$$

When the variance of $\mathbf{err}$ $\left(\sum_{m=1}^{Nd}[\mathbf{err}(m)^2/(Nd-1)]\right)$ has changed minimally from the previous step, then the final $\mathbf{err}(m)$ is considered to be the clean output $\mathbf{X\_out}(m)$ (ideally, S_o in equation 1) at the discrete time m. Because of the large dynamic range of the time series, better performance is typically achieved by first prewhitening each time series using a robust autoregressive (AR) filter (Chave and Thomson, 2004).

Applying the noise canceler to the Slave Lakes data gave generally satisfactory results. Figure 9 shows segments of noise-canceled magnetic-field signals along with the original (prewhitened) disturbed time series from Lake Tete d'Ours from the first-year survey. Tilt amplitudes (also prewhitened with the AR filter) for this site varied by up to 200 μrad in the time interval of August 13–15). The electric field within this interval was not affected by tilt, suggesting purely mechanical (noninductive) noise on the magnetic channels.

The noise canceler did not always fully succeed on magnetic time series having extreme disturbance levels, which usually occurred when the electric-field channels were also affected by tilt. Figure 10 shows such magnetic and electric time series from Aylmer Lake. This site was the shallowest deployment
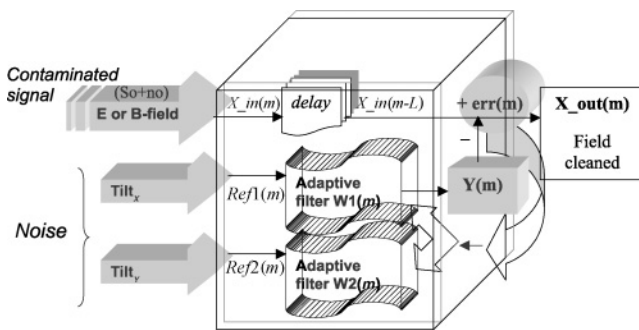

Figure 8. Schematic showing a time-domain adaptive filter to cancel tilt noise affecting the electric- or magnetic-field channels. The value $err(m)$ represents the residual uncorrelated signal, which is the clean output signal ($\mathbf{X\_out}$) after convergence has been reached.
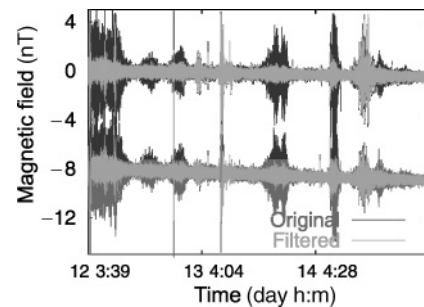

Figure 9. Prewhitened time series of original (dark gray curve) and noise-canceled horizontal components (light gray curve) for Lake Tete d'Ours in the measurement coordinate system. Curves are the magnetic B_x (top) and B_y (bottom) components at 106° and 196° from geographic north, respectively. The time window is during summer 1998 from August 13–15.

of the survey at 6 m, and both tilt components have similar amplitudes of up to 250 μrad. The adaptive correlation filter achieves only a partial reduction in the peak time-series amplitude, thus reflecting limited cancellation of the tilt-induced noise. Electric- and magnetic-field power spectra of noise-canceled peak segments demonstrate this, with values one to two orders of magnitude above the spectrum from a quiet segment (not shown).

After noise cancellation, the MT and magnetic transfer functions were estimated using the bounded-influence remote-reference algorithm of Chave and Thomson (2004). This algorithm eliminates highly disturbed segments automatically, provided there is minimal correlation between the corresponding electric E and magnetic B field components. Low correlation occurred when the B field was affected by tilt; therefore, MT impedances (the ratio of E to B field) estimated from time series after applying the noise canceler showed generally small improvements over the estimates without application of the filter, with the only notable differences at the shortest periods (<20 s; not shown). Figure 11 shows the magnetic transfer responses (the ratio of vertical to horizontal component of the B field) for Lake Tete d'Ours estimated from the original and the cleaned time series, showing differences between both curves even at periods greater than 10 s. In addition, the use of two-stage processing with a clean remote reference site to remove correlated noise from the input (magnetic-field) time series prior to estimating the transfer functions (Chave and Thomson, 2004) was needed to further reduce the bias at the shortest periods and for matching the curves obtained between the responses from the high- and low-sampling-rate data in the period range of 100 to 1000 s.

TILT AND WIND CORRELATION: EFFECT OF WIND WAVES

The Canadian Meteorological Service maintains four weather stations in the western sector of the MT array where most of the sites from the first-year survey are located. While the correlation scale of wind is typically a few meters and hence a statistical correlation of the wind from a distant station with local tilt is unlikely, correlation of intervals of high wind with large tilt variations suggests a causative relation. Further, such a relation is suggested by the occurrence of disturbed tilt intervals during the warm months when the lakes are not frozen and hence are subject to the generation of wind waves.

We analyzed August 1998 and September 1999, periods when the high-sampling-rate data from the two year-long surveys were recorded. During August 1998, the average wind direction at each weather station when the wind speed exceeded 15 km/hour was spatially homogeneous and south–southwestly, with mean values ranging from 23 to 27 km/hour. In September 1999, the wind direction was more to the north (i.e., a southerly wind) with average wind speed very similar to that from August of the previous year.

Highly disturbed tilt events consistently coincided with high wind. This indicates wind was a driving force (direct or indirect) for water movements at the bottom of the lakes where the MT instruments were located. The highly disturbed segments with the largest tilt amplitude occurred when wind speeds were extremely high (usually exceeding 30 km/hour), even for sites set below 20 m depth. Usually a time delay of a few hours was observed between peak wind and peak tilt. Peak winds (up to 55 km/hour) typically lasted for about 3 hours, followed by a calmer interval of a few hours before high winds recurred. However, tilt continued to be consistently disturbed despite the sequence of low and high wind speeds, usually lasting for up to two to three days (see data from Lake Tete d'Ours in Figure 12).

Intuitively, instrument motion and/or local induction by wind-driven surface gravity waves are the most likely mechanisms for the observed tilt disturbance. Proving this would require data and models that are not readily available — notably, wind data distributed around each lake, depth
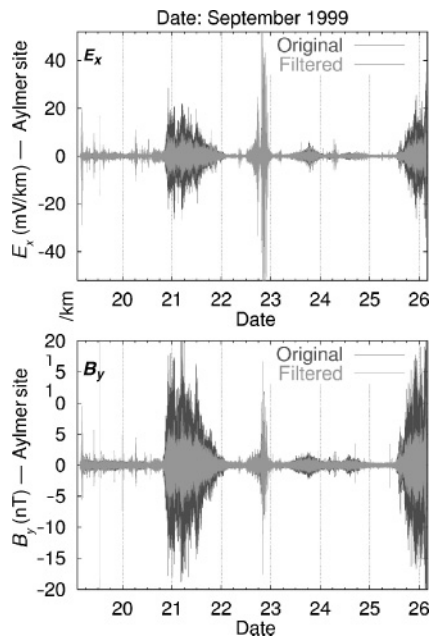

Figure 10. Prewhitened time series of original (dark gray curve) and noise-canceled horizontal components (light gray curve) for Aylmer Lake in the measurement coordinate system. Graphs from both (top) the electric (E_x) and (bottom) the magnetic (B_y) components at $185°$ and $230°$ from geographic north, respectively. The time window is during fall 1999 from September 19–26.
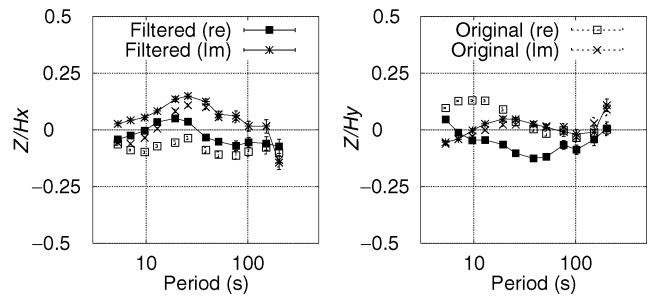

Figure 11. Magnetic transfer functions for Lake Tete d'Ours estimated with a bounded-influence algorithm (Chave and Thomson, 2004). Symbols joined with lines are from cleaned (filtered) time series, while symbols alone are from the original time series without application of the noise canceler. Real parts are square symbols, and imaginary parts are asterisks. Vertical component of the magnetic field is Z_y; horizontal component are H_x (left) and H_y (right) in the measurement coordinate system, as in Figure 10.

information about the lakes, and measurements of the electrical conductivity of lake water. It would also require a sophisticated model of the mechanical response of the lake-bottom instruments to water motion over a range of spatial scales and frequencies. None of these are available; hence, we rely on simple bounds on the water motion produced by wind-induced waves and on the response of a cylindrical body to wave motion.

Gravity-wave response to wind forcing occurs over a continuum of frequencies, depending strongly on fetch and water depth and on the wind growth. Wave prediction models such as ACES (Veri-Tech, 2005) are available for coastal areas; they can be restricted in depth and laterally based on finite-water-depth linear theory, though these are only approximately applicable to the more tightly bounded geometry of the Slave lakes. Assuming wind speeds between 25 and 37 km/hour lasting for 3 hours or longer (Figure 12), our estimates of wave periods and wave amplitudes were obtained from this algorithm for combinations of input variables. The dominant variables were fetch (2–30 km) and lake depth (10–50 m); of secondary importance was the differential temperature between the air/water interface (a few degrees). Wave periods between 1 and 2 s and amplitudes of 0.2 to 0.4 m for the smallest lakes (fetch <7 km) and around 3- to 5-s periods and 0.4- to 0.6-m amplitude for the largest Slave lakes (fetch of 10 to 20 km) were obtained.

Wave angular frequency ω and wavenumber k for surface gravity waves were related through the finite-water-depth dispersion relation: $\Omega^2 = gk \tanh(kd)$, where g is the acceleration of gravity and d is the water depth. At a wave period of 4.5 s
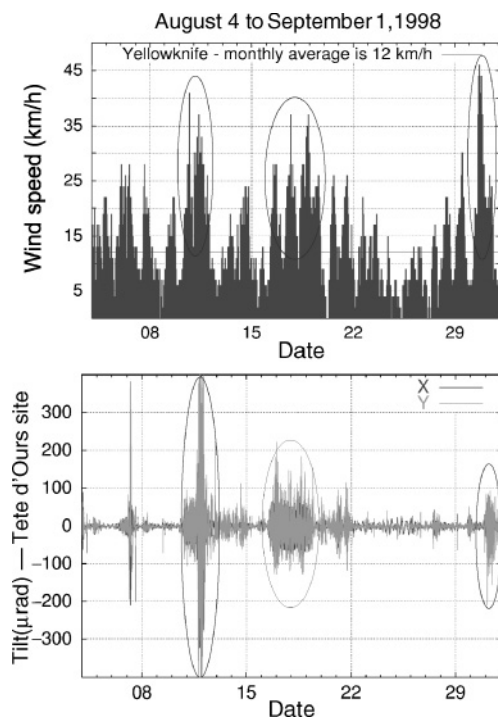

Figure 12. (Top) Hourly wind speeds at Yellowknife during August 1998 and (bottom) the two components of prewhitened tilt (microradians) from Lake Tete d'Ours recorded during that same month. Ovals denote the correlation between wind peaks and highly disturbed tilt. Location of the sites is shown in Figure 2.

and a water depth of 20 m, the wavenumber is 0.19887, so that the wavelength is 31.6 m. The deepwater approximation is obtained when $kd > \pi$, so that $w^2 \sim gk$, implying that deepwater theory is appropriate for the lakes, assuming maximum wave periods of about 5 s if wind growth is the dominant force for surface gravity wave generation during high wind events. At a short wave period of 1 s (more likely at the smaller lakes) and water depth of 10 m, the wavelength is 2 m; hence, the deepwater approximation becomes even more valid. At longer wave periods, deep-water theory does not apply.

The deep-water motion (orbital velocity v) from surface gravity waves decays exponentially with depth z according to $v = \omega A e^{-kz}$, where A is the surface-wave amplitude. Assuming a wave period of 3 s at an amplitude of 0.6 m, the horizontal water particle displacement is 1.2×10^{-8} cm/s on a lake bed of 50 m depth (the deepest instrument deployment), 0.0074 cm/s at 20 m depth (the general instrument depth), and 4 cm/s at 6 m depth (the shallowest deployment). Hence, surface gravity wave-induced instrument motion may well account for the tilt oscillations.

Further insight can be obtained from the observation that the tilt motion is typically three to four times larger across the magnetometer cylinder (*y*-axis) compared to along the cylinder (*x*-axis). This is consistent with the higher force needed to lift the larger cross-sectional area along *x* than is needed for lifting (or rotating, in this case) along its cylinder diameter (*y*). Karman vortex shedding of the magnetometer cylinder can be estimated from the nondimensional Strouhal number *S*, which is typically 0.22 in laminar flows (e.g., Newman, 1997). The value *S* is the product of vortex frequency and cylinder diameter divided by water velocity. At a dominant period of 4.5 s and for a cylinder diameter of 23 cm, the water velocity would have to be 23 cm/s to produce $S \sim 0.22$. This is much higher than the velocities estimated for surface gravity waves and is also higher than any other likely disturbance. For example, internal waves for typical stratified lakes have estimated velocities between 1 and 10 cm/s at the lake bed (H. Nepf, personal communication, 2003). Unless the instrument is excited in one of the modes of its natural resonance frequency by the water mass passing by the cylinder, vortex shedding does not appear to be an explanation for the observed tilt.

Finally, we note that two sites never displayed large summertime tilt variations: Duncan and Kuuvik. The former is located close to Yellowknife, where the wind speed was lower than at northern locations. Further, its fetch is negligible under the direction of strong wind measured at that time, suggesting that surface wave generation is weak. An explanation for the behavior of the very small Lake Kuuvik is lacking.

MOTIONAL ELECTRIC FIELD FROM SURFACE GRAVITY WAVES

We showed earlier that some sites displayed electric- as well as magnetic-field variations correlated with tilt (Figure 10), suggesting EM induction by water motion.

The electric-field amplitude induced by a moving medium (water, in this case) is given by Ohm's law:

$$\mathbf{E'} = \mathbf{E} + \mathbf{v} \times \mathbf{B} \qquad (6)$$

(e.g., Larsen, 1971), where $\mathbf{E'}$ is the electric field in a reference frame moving at velocity $\mathbf{v}$, $\mathbf{E}$ is the *E* field in a fixed reference

frame, and **B** is the steady geomagnetic field. This provides the basic principle for estimation of motion-induced electric and magnetic fields within the ocean and lakes.

The equation for the electric and magnetic fields induced by a plane progressive gravity wave in a flat-bottomed water body of uniform depth has been estimated by several authors (e.g., Weaver, 1965; Larsen, 1971). Assuming the thickness of the conductive water layer, sedimentary cover, and lithosphere to be small compared to the wavelength of the incident field and a negligible conductivity for the air and lithosphere (underlain by a conductive mantle), Larsen (1971) derives the motional electric field induced by surface gravity waves. Assuming the Slave lakes may be approximated by a model with a uniform water depth and an infinite lateral extent like the ocean, the motional horizontal electric and vertical magnetic fields can be estimated by using the formula derived by Larsen (1971; his equations 17 and 23). If we consider fresh-water conductivity to range from 0.1 to 0.01 $\Omega^{-1}\mathrm{m}^{-1}$, subject to wind waves of a period up to 5 s and wave amplitude up to 0.8 m with uniform water depth ranging from 7 to 10 m, the horizontal electric field reaches a magnitude of nearly 0.2 mV/km and the vertical magnetic field amplitude is up to 0.01 nT.

These estimates cannot explain the effect of electric-field noise observed in the instruments deployed at 6 m depth in the large Aylmer Lake and at 10 m depth in the small Newbigging Lake, where the differences between a calm and a disturbed *E* field were on the order of 10 to 15 mV/km for Aylmer Lake and ~8 mV/km for Newbigging. This suggests that the approach of a flat bottom for the Slave lakes is not appropriate and/or the water motion in these lake beds is not caused solely by surface gravity waves from wind-driven forces. Considering wave periods beyond 5 s would cause the breakdown of Larsen's (or Weaver's) equations, as these are based on intermediate and deepwater wave theory and are limited by the depth of the deployment (10 m) in this case.

For *E*-field amplitudes generated directly from the instrument motion, a simple calculation shows that the electrodes must move at improbably high speeds (|**v**|) of around 20 cm/s for **v** × **B** (equation 6) to be comparable to the *E*-field disturbance observed. Such a speed is similar to the laminar flow velocity estimated from vortex shedding of the magnetometer. Is that a mere coincidence, or is it because the instrument oscillated at some natural resonance frequency mode by the water motion? To answer this question will require data not available at present.

DISCUSSION AND CONCLUSIONS

We have shown from magnetotelluric surveys performed on the bottom of lakes of the Slave craton that magnetic-field data were disturbed by instrument motion that also registered in measurements of tilt. In some cases, the electric field may also have been affected by EM induction generated by water motion.

The disturbances in the time series were highly correlated with tilt with a relatively consistent dominant period of around 4 s, regardless of the depth and size of the lakes where the instruments were deployed. The magnetic- and sometimes electric-field channels can be pretreated with an adaptive correlation cancellation filter using the two components of tilt as a reference signal. The method satisfactorily reduces the

noise in the EM data under most circumstances. Exceptions are seen for some sites where the electric-field noise was not negligible and hence there was correlated noise in the electric and magnetic channels. In this case, information on rotation of the instrument about the local vertical may be needed for optimal noise cancellation. In addition, a two-stage, bounded-influence processing algorithm with a clean remote reference site was generally required for processing the filtered time series to obtain stable MT responses.

To reduce the instrument motion, it would be desirable to install the magnetometer in a solid package with a geometry that minimizes vortex shedding and thereby limits the oscillatory forces on it. In general, this means placing instruments close to the bottom with a minimum of buoyancy and the center of buoyancy located close to the center of mass of the anchor. In addition, a spherical case with small dimples like a golf ball can help reduce vorticity, although at the cost of increased drag force. Drag force on the instrument can be reduced using a stiffer and heavier base (a rigid tripod of ~25 kg was used in this survey). These considerations are of particular importance in coastal regions where seabed currents are expected to be strong, for which tilt-induced EM fields from the water movement could be significant.

REFERENCES

Bastani, M., and L. B. Pedersen, 1997, The reliability of aeroplane attitude determination using the main geomagnetic field with application to tensor VLF data analysis: Geophysical Prospecting, **45**, 831–841.

Chave, A. D., and D. J. Thomson, 2004, Bounded influence estimation of magnetotelluric response functions: Geophysical Journal International, **157**, 988–1006.

Filloux, J. H., 1987, Instrumentation and experimental methods for oceanic studies, *in* J. A. Jacobs, ed., Geomagnetism, vol. 1: Academic Press, 143–248.

Jones, A. G., P. Lezaeta, I. J. Ferguson, A. D. Chave, R. L. Evans, X. Garcia, and J. Pratt, 2003, The electrical structure of the Slave craton: Lithos, **71**, 505–527.

Larsen, J. C., 1971, The electromagnetic field of long and intermediate water waves: Journal of Marine Research, **29**, 28–45.

Newman, J. N., 1997, Marine hydrodynamics: MIT Press.

Petitt Jr., R. A., A. D. Chave, J. H. Filloux, and H. H. Moeller, 1994, Electromagnetic field instrument for the continental shelf: Sea Technology, **35**, 10–13.

Veri-Tech Inc., 2005, ACES software, http://veritechinc.net/products/cedas/ACESmodel.htm (accessed March 2005).

Weaver, J. T., 1965, Magnetic variations associated with ocean waves and swell: Journal of Geophysical Research, **70**, 1921–1929.

Widrow, B., and S. D. Stearns, 1985, Adaptive signal processing: Prentice-Hall, Inc.